Further Exploration into the Bistable Behavior of Caspase-Initiated Apoptosis

Ainsley Lai, Xi Liang, Ayush Sharma, Agastya Pulapaka

December 2022

Contents

1 Introduction

1.1 Caspase-Initiated Apoptosis

Apoptosis is a biological process in which cells undergo programmed cell death that is triggered by the presence of noxious agents or hormonal signaling [Elm07]. This mechanism, in opposition to the acute death process called necrosis, is characterized by safe, contained degradation of cellular components as to avoid damage to the healthy surrounding tissues. The process of apoptosis is heavily regulated, most notably by the caspase-cascade signaling pathway, which consists of aspartate-specific cysteine proteases. Caspases are zymogens, which are proteins that are excreted in an inactive form (pro-caspases) and are activated by a biochemical change after intaeraction with another protein [FHRSC05]. Figure 1 illustrates a simplified map of the protein interactions involved in invoking apoptosis, where CX becoming CX^* indicates the transition from a pro-caspase to active caspase. It is noteworthy that this map does not include all 12 known caspases in human tissue [SVG+04]. It is also important to note that caspase 8 and caspase 3 are the most heavily regulated, integral proteins in this pathway. Pro-caspase 8 is activated by a cell stress signal, and caspase 8 then activates pro-caspase 3. Caspase 3 is the key regulator that when at a sufficiently high concentration, can trigger the apoptotic process.

1.2 Bistability of the Apoptotic State

Bistability in the context of biological systems refers to the ability for a defined cellular process to attain two distinct steady states [AMVL+21]. In other words, the initial conditions of the various protein concentrations of the process dictate the long-term behavior of the system such that it can only reach two different states. In the context of apoptosis, bistability refers to the ability for the cell to achieve a life state, in which apoptosis is inhibited, or an apoptotic state. In terms of long-term behavior, the absence of active caspase 3 is indicative of the life state, whereas notable, stable

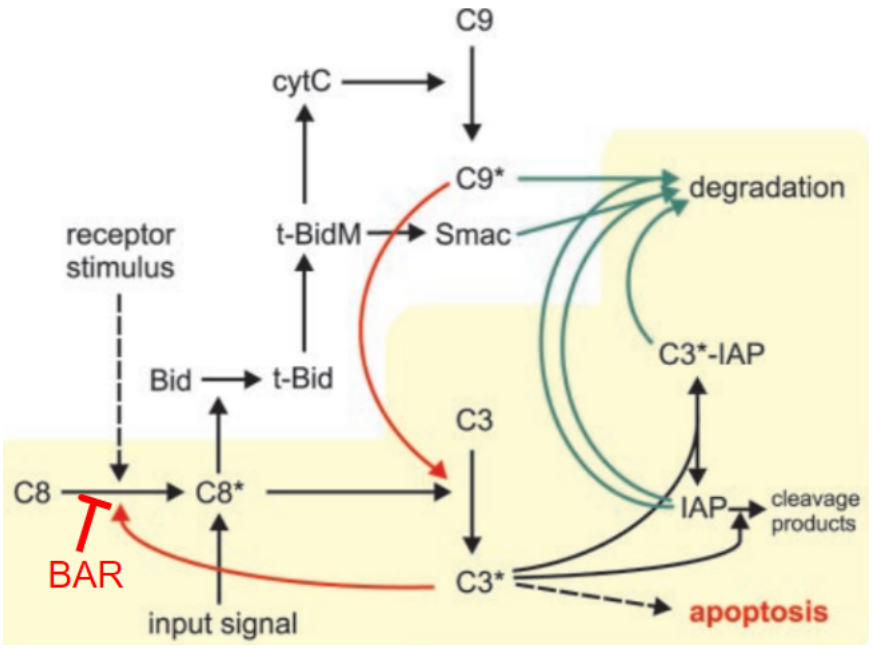

Figure 1: The basic outline of the apoptotic pathway for our model. For our novel results, focus was given to the pathway starting at C8*, that ultimately activates C9 into C9*.

concentrations for caspase 3 of around 5000 molecules/cell describes the apoptotic state [ECG+04]. This bistability phenomenon is illustrated in Figure 2, where low C8* input eventually results in a stable, inactive C3* life steady state, and sufficient C8* input results in a stable, non-zero amount of C3* indicating the apoptotic steady state. When the dynamics of the caspase-cascade signaling system are modeled and implemented, the investigation of this bistable phenomenon can provide insight into the behavior of this complex pathway, and the results can be interpreted under a biological context to compare whether the conclusions are reasonable and exhibited in an experimental setting.

2 Detailed Description of Model Equations

The original paper presented by Eissing et al [ECG+04] derives a system of ordinary differential equations 1 for the model from the set of selected apoptotic reactions using the law of mass action. Two different model structures are tested in the original study.

The basic model based on the reactions highlighted in light yellow background in Figure 1 does not include reactions involving molecule BAR and only contains equations 1a-1f and does not have $-v_{11}$ term in Equation 1b. The extended model adds reactions related to BAR in Figure 1 and applies all equations in 1. The v values in each equation of the equation set 1 represent the overall reaction rates of individual reactions, and their calculations are shown in equation set 2, where the values of parameters k are the reaction rate constants that quantifies the rate and direction of the chemical reactions. It is important to note that most k values with negative subscript are not the reaction rate constants: only k_{-3} and k_{-11} are the rate constants for the reverse reactions of corresponding reactions with k_3 or k_{11}, the rest of nonzero k's with negative subscript are the basic production rate of different molecules. For example, k_{-8} represents the production rate of IAP molecules shown in Equation 2h.

$$\frac{d[C8]}{dt} = -v_2 - v_9 \tag{1a}$$
$$\frac{d[C8^*]}{dt} = v_2 - v_5(-v_{11}) \tag{1b}$$
$$\frac{d[C3]}{dt} = -v_1 - v_{10} \tag{1c}$$
$$\frac{d[C3^*]}{dt} = v_1 - v_3 - v_6 \tag{1d}$$
$$\frac{d[IAP]}{dt} = -v_3 - v_4 - v_8 \tag{1e}$$
$$\frac{d[C3^* \sim IAP]}{dt} = v_3 - v_7 \tag{1f}$$
$$\frac{d[BAR]}{dt} = -v_{11} - v_{12} \tag{1g}$$
$$\frac{d[C8^* \sim BAR]}{dt} = v_{11} - v_{13} \tag{1h}$$

The initial concentrations of the molecules and the values for parameters k adopt the numbers from the experiments and past reports. The paper itself does not specify the initial concentrations of all molecules but mentions the average concentrations of some proteins and the various C8 levels in different reports, so we did some research, modified and tested a few sets of values for our own model. The used values in our model are

shown in Code in Section 6. The values of k are presented by the original paper and are shown in Table 1.

$$v_1 = k_1[C8^*] \cdot [C3] \tag{2a}$$

$$v_2 = k_2[C3^*] \cdot [C8] \tag{2b}$$

$$v_3 = k_3[C3^*] \cdot [IAP] - k_{-3}[C3^* \sim IAP] \tag{2c}$$

$$v_4 = k_4[C3^*] \cdot [IAP] \tag{2d}$$

$$v_5 = k_5[C8^*] \tag{2e}$$

$$v_6 = k_6[C3^*] \tag{2f}$$

$$v_7 = k_7[C3^* \sim IAP] \tag{2g}$$

$$v_8 = k_8[IAP] - k_{-8} \tag{2h}$$

$$v_9 = k_9[C8] - k_{-9} \tag{2i}$$

$$v_{10} = k_{10}[C3] - k_{-10} \tag{2j}$$

$$v_{11} = k_{11}[C8^*] \cdot [BAR] - k_{-11}[C8^* \sim BAR] \tag{2k}$$

$$v_{12} = k_{12}[BAR] - k_{-12} \tag{2l}$$

$$v_{13} = k_{13}[C8^* \sim BAR] \tag{2m}$$

For better understanding, we will briefly walk through the derivation of Equation 2a, connecting the concepts of v and k together and incorporating it into corresponding equations in equation set 1. It is important to note that the other equations also follow similar derivation processes. Considering the reaction

$$C8^* + C3 \xrightarrow{k_1} C8^* + C3^*$$

that an activated caspase 8 ($C8^*$) cleaves and activates one caspase 3 ($C3$) to the active form ($C3^*$) with a rate constant k_1, the depletion rate of the reactant $C3$ and the production rate of the product $C3^*$ are the same and proportional to the concentrations of reactant $C3$, the concentration of the enzyme $C8^*$, and the rate constant k_1. Thus,

	Value	Unit		Value	Unit
k_1	$5.8 \cdot 10^{-5}$	$cell \cdot min^{-1} \cdot mo^{-1}$	k_{-1}	0	
k_2	10^{-5}	$cell \cdot min^{-1} \cdot mo^{-1}$	k_{-2}	0	
k_3	$5 \cdot 10^{-4}$	$cell \cdot min^{-1} \cdot mo^{-1}$	k_{-3}	0.21	min^{-1}
k_4	$3 \cdot 10^{-4}$	$cell \cdot min^{-1} \cdot mo^{-1}$	k_{-4}	0	
k_5	$5.8 \cdot 10^{-3}$	min^{-1}	k_{-5}	0	
k_6	$5.8 \cdot 10^{-3}$	min^{-1}	k_{-6}	0	
k_7	$1.73 \cdot 10^{-2}$	min^{-1}	k_{-7}	0	
k_8	$1.16 \cdot 10^{-2}$	min^{-1}	k_{-8}	464	$mo \cdot cell^{-1} \cdot min^{-1}$
k_9	$3.9 \cdot 10^{-3}$	min^{-1}	k_{-9}	507	$mo \cdot cell^{-1} \cdot min^{-1}$
k_{10}	$3.9 \cdot 10^{-3}$	min^{-1}	k_{-10}	81.9	$mo \cdot cell^{-1} \cdot min^{-1}$
k_{11}	$5 \cdot 10^{-4}$	$cell \cdot min^{-1} \cdot mo^{-1}$	k_{-11}	0.21	min^{-1}
k_{12}	10^{-3}	min^{-1}	k_{-12}	40	$mo \cdot cell^{-1} \cdot min^{-1}$
k_{13}	$1.16 \cdot 10^{-2}$	min^{-1}	k_{-13}	0	

Table 1: The values for simulation parameter k in the model implemented by the original paper (mo = molecules).

the absolute value of the changes of concentrations of $C3$ and $C3^*$ in this reaction can be deduced to the equation $v_1 = k_1[C8^*] \cdot [C3]$. Because the concentration of $C3$ decreases while the concentration of $C3^*$ increases in this reaction, Equation 1c has the term $-v_1$ and Equation 1d has the term v_1.

With all these ODE equations and initial conditions, it is possible to use ODE solvers to get the concentrations of these molecules through time and run multiple simulations to produce viable results.

3 Reproduction of Results in Paper

Reproduction of Eissing's Fig. 4, which displays the $C3^*$ amount over time with varying initial $C8^*$ concentrations, begins with the simulation of the dynamical system. For this, usage of the python package, SciPy, was used to solve the system over the timespan presented by Eissing et al [ECG+04].

3.1 Original Model Elements

For recreating the figure, identification of the various components of the model serves to expedite the process. We note that the dynamical system is abstracted with various v

terms, each incorporating some k term(s). Both of these components can be determined by literature, the law of mass action, and stability analysis.

To give further exposition on the determination of the k terms, Eissing references other literature and employs analytical techniques, namely stability analysis, using Mathematica to determine k values. This uses the general method of finding steady states/fixed points using nullclines and the Jacobian for stability. By testing different values in the Jacobian, Eissing is able to test which values create proper, realistic stable steady states: one for the life steady state and another for the apoptotic steady state.

For initial concentrations/conditions, reported concentrations from other literature are 18000, 120000, and 18000 molecules per cell for caspase 8, caspase 3, and IAP, respectively [SJS+98] [SBB+02]. When simulating these concentrations, it becomes clear that the result does not match Eissing's shown figure. Instead, we switch the values for caspase 8 and 3, giving a ratio and order of magnitude similar to those found in HeLa cells, another set of proposed initial concentrations. Since C8* acts as the input signal that Eissing varies, we use the same range of values from 0 to 3000.

From the figure, it is also apparent that the system is simulated over a timespan of approximately 1500 minutes (or equivalently around one day). It is possible that this timespan was chosen to give ample time to model the apoptosis process while remaining short enough to not disturb the simple model. If a longer timespan were to be chosen, the model may need to consider other bodily factors that would come into play, further complicating the proposed model. From that point on, the derived system is easy enough to implement.

3.2 Reproduction Methods and Results

With the equations, interaction terms and reaction rates clearly defined, creating the dynamical system is straightforward. Values for the reaction rates, k, can be stored in an array that is passed into a function for our dynamical system. Said function will serve as the engine for our model as it contains the 8 model equations. By defining

interaction terms within our ODE function, we're able to write our equations in a way identical to the original paper. Once these things have been set up, we're able to simulate our systems with the correct initial conditions. Code for creating this figure can be found in section 6.

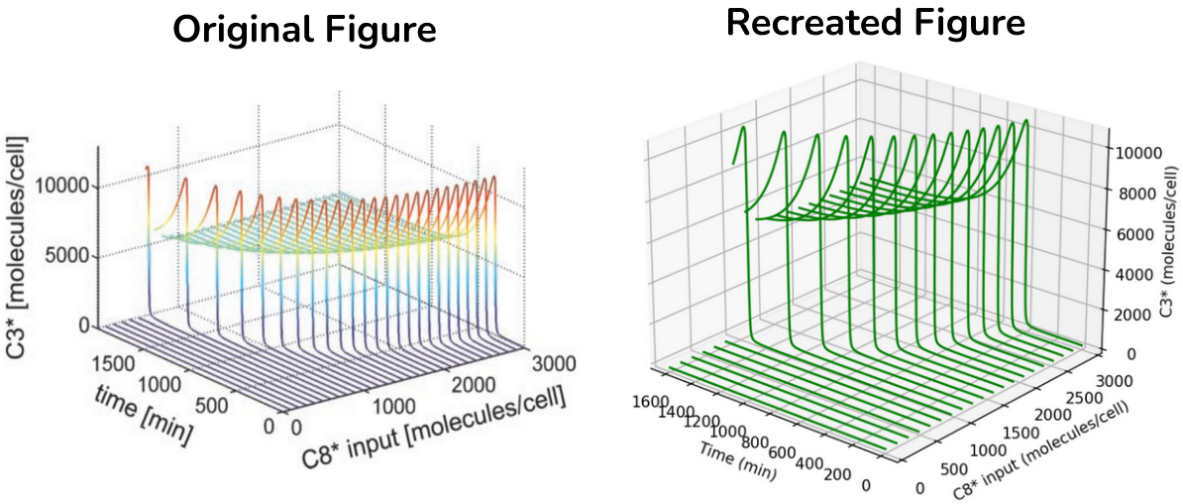

Figure 2: Reproduction of Figure 4 from Eissing et al [ECG+04]

In the recreated figure, we can note that the bistability that the original paper brings light to is retained in our code with the right values where the apoptotic state flattens out near $C3^* \approx 5000$, starting around $C8^*(t = 0) = 1000$. This figure is the driving plot of the studied apoptosis model as it illustrates the bistability of the system as a result of a varying input signal.

4 Novel Results

4.1 Extension of the Original Model

Our novel question revolved around investigating the effects of other factors in the caspase-activation model for apoptosis. To that end, a simple extension was to include one of the caspases, Caspase-9, that was involved in the system, that had previously been neglected by the original authors for simplicity.

C9 presents behavioral similarities to both C8 and C3, the caspases previously

studied. C9 and C8 share the characteristic of initiating the apoptosis reactions once in their activated state, however, a key difference to note is that C8 $\rightarrow$ C8* occurs due to stimuli external to the cell, whereas C9 $\rightarrow$ C9* occurs due to an internal stimulus in the form of a lengthy series of chain reactions, initiated by C8. The activated C9 then, in turn, increases the production of C3* from C3, aiding in the activation process. Interestingly, while having differing functions within the cell, C3* and C9* share the same inhibiting protein, i.e, IAP. This is an important distinction between C9 and C8, since C8* was inhibited by an entirely different protein, i.e., BAR. The interactions of C9 with the system are illustrated in Figure 1.

These effects of C9 and C9* on the overall system led to the alterations in the pre-existing biochemical reactions of the system and entirely new reactions involving C9. These altered and new reactions then led to the definition of new v terms, and new differential equations, as well as altering previous differential equations. These new variables are listed below:

$$v_{14} = k_{14}[C9] \cdot [C8^*] \tag{3a}$$

$$v_{15} = k_{15}[C9] - k_{-15} \tag{3b}$$

$$v_{16} = k_{16}[C9^*] \cdot [IAP] - k_{-16}[C9^* \sim IAP] \tag{3c}$$

$$v_{17} = k_{17}[C9^*] \tag{3d}$$

$$v_{18} = k_{18}[C9^* \sim IAP] \tag{3e}$$

$$v_{19} = k_{19}[C3] \cdot [C9^*] \tag{3f}$$

The new and modified equations, including new variables are given below:

$$\frac{d[C9]}{dt} = -v_{14} - v_{15} \tag{4a}$$
$$\frac{d[C9^*]}{dt} = v_{14} - v_{16} - v_{17} \tag{4b}$$
$$\frac{d[C9^* \sim IAP]}{dt} = -v_{16} - v_{18} \tag{4c}$$
$$\frac{d[C3]}{dt} = -v_1 - v_{10} - v_{19} \tag{4d}$$
$$\frac{d[C3^*]}{dt} = v_1 - v_3 - v_6 + v_{19} \tag{4e}$$
$$\frac{d[IAP]}{dt} = -v_3 - v_4 - v_8 - v_{16} \tag{4f}$$

We shall analyze the bistability of this now 11 variable system, 3 new variables have been added, namely, the concentrations of C9, C9* and C9* ∼ IAP. This analysis will be performed using the same method adopted by the original authors.

4.2 Parameters of the Extended Model

For analyzing the behavior of the extended model, the first step was to set values for the new rate constants (the k parameters in the new equations), as well as to set an initial value for the concentration of C9. Through studying the literature, several initial conditions for the concentration of C9 were found, ranging from 1nM to 1μM. In order to obtain sensible values for the new k parameters, a computational approach proved incoherent and inconclusive. Thus, a more analytical and theoretical approach was employed. The v variables used to represent the biochemical reactions were segragated into different types, depending on the nature of the reaction they represented. For example, v_1 and v_{14} have a similar structure, hence they would be of the same type, and their respective k parameters would be comparable. Additionally, the units of the k variables also helped in identifying similar v variables and k parameters. Using this method, a reasonable assumption could be made regarding the **order of magnitude of the k parameters, and their units**. After determining the orders of magnitude,

several specific values were tested until the system attained the desirable behaviour. The specific k values used are listed in the table below:

	Value	Unit		Value	Unit
k_{14}	10^{-5}	$cell \cdot min^{-1} \cdot mo^{-1}$	k_{-14}	0	
k_{15}	$1.8 \cdot 10^{-2}$	min^{-1}	k_{-15}	3	$mo \cdot cell^{-1} \cdot min^{-1}$
k_{16}	$3.4 \cdot 10^{-4}$	$cell \cdot min^{-1} \cdot mo^{-1}$	k_{-16}	3	min^{-1}
k_{17}	$5.8 \cdot 10^{-3}$	min^{-1}	k_{-17}	0	
k_{18}	$7 \cdot 10^{-3}$	min^{-1}	k_{-18}	0	
k_{19}	$2 \cdot 10^{-5}$	$cell \cdot min^{-1} \cdot mo^{-1}$	k_{-19}	0	

Table 2: The values for added rate constant k used in the extended model (mo = molecules).

4.3 Simulating the Extended Model and Results

The extended model was then simulated using the parameter vales enumerated above, similar to how the simulation of the original model was done. Since the initial value of C9 was spread across a wide range, we took three distinct initial values to see the effect on the overall system.

From the simulations conducted at varying initial values of C9, it can be seen that the bistable behavior of the system is maintained throughout, regardless of the initial value. However, the threshold value for C8* input that results in a stable apoptotic state reduces with an increase in the initial value. This is a rather intuitive result, since C9 adds to the amount of C3* present in the system, which is the direct cause of apoptosis.

Fig 3.1: C9 = 600 molecules/cell

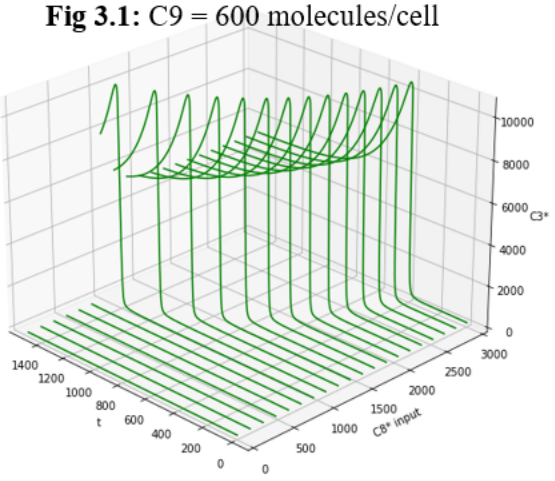

Fig 3.2: C9 = 10,000 molecules/cell

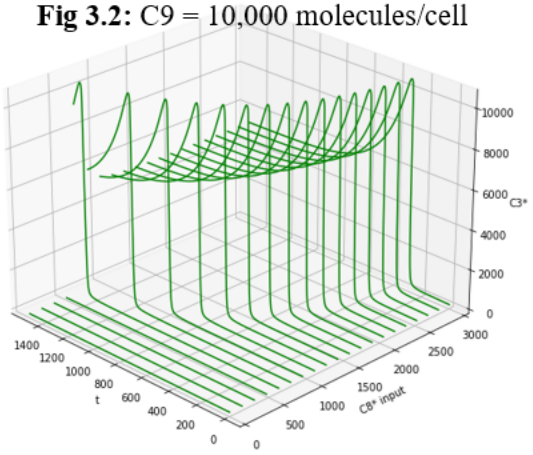

Fig 3.3: C9 = 100,000 molecules/cell

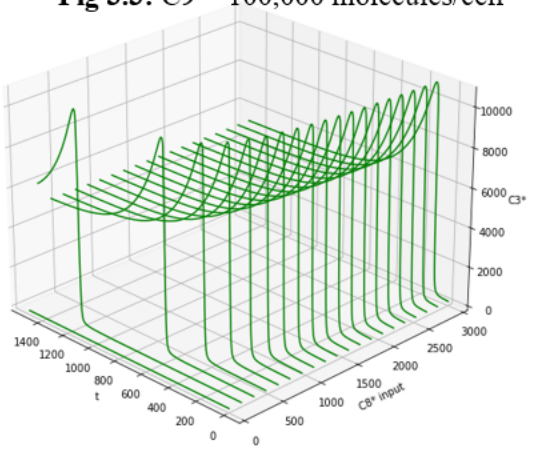

Figure 3: The bistability plot of C8* vs $C3^*$ at an initial value of **(3.1)** C9 = 600. Such a low initial value has little to no effect on the behavior of the system. Bistability is evident, and the original threshold value of $\sim$ 75 mol of C8* has changed a negligible amount. **(3.2)** C9 = 10000. Such an initial value has a noticeable effect on the behavior of the system. Bistability is evident, and the original threshold value of $\sim$ 75 mol of C8* has reduced to a lower value. **(3.3)** C9 = 100000. Such a high initial value has a strong effect on the behavior of the system. Bistability is evident, and the original threshold value of $\sim$ 75 mol of C8* has reduced to a much lower value.

5 Conclusions and Discussion

5.1 Conclusions From Original Work

The original paper set out to investigate the conditions required for bistability of caspase activated apoptosis. By analyzing the reaction rates which resulted in the desired kinetics of the reactions in the system, the authors were able to identify ranges of values for which bistability was possible. A deeper look was then taken into the relationship between C3, C8, and their regulatory proteins, IAP and BAR. The system exhibited bistability through a wide range of $C8^*$ inputs, from 0 to 3000, with a stable apoptotic state beginning around a threshold value of 75 molecules per cell. This threshold value seems optimal for a process such as apoptosis, as it is large enough to prevent random fluctuations in concentration from initiating apoptosis, and low enough to be attained at a quick rate after an initial signal has been passed into the system.

5.2 Conclusions From Novel Work

Our novel work set out to investigate the effects of C9 on the apoptotic system. By using the same analytical tools as Eissing et al [ECG+04], we were able to understand that C9 does not seem to have a strong effect on the bistable nature of the system. i.e, at parameter values where bistability held before C9 was introduced, it held after C9 was introduced, and for parameter values where bistability failed to hold, the introduction of C9 had no mitigating effect.

Where C9 does have an effect on the system, however, is the rapidity of apoptosis. In other words, the time taken from the system receiving an external signal which begins the activation process of C8, to $C3^*$ being released is reduced by the presence of C9. In reference to biological analogue, this result is reasonable. Given that in an experimental setting, apoptosis is very difficult to stop once the mechanism has begun [Elm07], it would be plausible that the introduction of another caspase regulator would enhance the probability of activating apoptosis in the signaling process. While this is a

promising result for situations where apoptosis must occur at a rapid rate, the negative impact must also be understood. The extremely low threshold value for high initial conditions of C9 may point to an exceedingly sensitive and volatile system, one where apoptosis could occur due to even a small fluctuation in $C8^*$ concentrations. This is not ideal for a biological system, since these types of small fluctuations are common in nature.

5.3 Further Directions

In order to understand the phenomenon of bistability in caspase-activated apoptosis, it is a good idea to analyze the core constituents that govern the system. While our novel research introduced a new element in the form of C9, work aiming for a deeper understanding of the relationship between the regulatory proteins IAP and BAR, and their effects on bistability, would help shed some new light on the biological problem at hand.

Because the current bistable behavior of the system mainly relies on the range of parameter k's, modifying the k's certainly helps us to investigate more into the dynamics of the system. In biological interpretation, changes in k's can be regarded as mutations occurring in corresponding proteins that lead to changes in reaction rates, which is quite common in the natural world. By modifying k's, we may simulate situations for uncommon conditions, such as in the case where one or a few mutations occurring in the apoptotic pathway. However, the potential risk for such change is also evident: the current bistable behavior may break. More stable states may arise, and they may become unrealistic, being complex or negative. Careful analysis is necessary to ensure the further extended model is biologically significant and indeed produces viable results with reasonable physical meanings.

6 Appendix

6.1 Code used for recreation of the original figure

```
import numpy as np
import scipy.integrate as inte
import sympy as sp
import matplotlib.pyplot as plt


# initialization of ODE functions
def odes(t, x, k, k_neg):
    v1=k[0]*x[1]*x[2]
    v2=k[1]*x[0]*x[3]
    v3=k[2]*x[3]*x[4]-k_neg[2]*x[5]
    v4=k[3]*x[3]*x[4]
    v5=k[4]*x[1]
    v6=k[5]*x[3]
    v7=k[6]*x[5]
    v8=k[7]*x[4]-k_neg[7]
    v9=k[8]*x[0]-k_neg[8]
    v10=k[9]*x[2]-k_neg[9]
    v11=k[10]*x[1]*x[6]-k_neg[10]*x[7]
    v12=k[11]*x[6]-k_neg[11]
    v13=k[12]*x[7]


    dC8dt = -v2-v9 #C8
    dC8sdt = v2-v5-v11 #C8*
    dC3dt = -v1-v10   #C3
    dC3sdt = v1-v3-v6 #C3*
```

```
    dIAPdt = -v3-v4-v8 # IAP
    dIAPsdt = v3-v7 # C3*~IAP
    dBARdt = -v11-v12 # BAR
    dBARsdt = v11-v13 # C8*~BAR

    return np.array([dC8dt,dC8sdt,dC3dt,dC3sdt,
                     dIAPdt,dIAPsdt,dBARdt,dBARsdt])

# values like k_1, ...
k = np.zeros(13)
k[0]=5.8*(10**-5)
# k[0]=5.8*(10**5)
k[1]=10**-5
k[2]=5*(10**-4)
k[3]=3*(10**-4)
k[4]=5.8*(10**-3)
k[5]=5.8*(10**-3)
k[6]=1.73*(10**-2)
k[7]=1.16*(10**-2)
k[8]=3.9*(10**-3)
k[9]=3.9*(10**-3)
k[10]=5*(10**-4)
k[11]=10**-3
k[12]=1.16*(10**-2)

k_neg = np.zeros(13)
k_neg[2]=0.21
k_neg[7]=464
```

```
k_neg[8]=507
k_neg[9]=81.9
k_neg[10]=0.21
k_neg[11]=40

# tspan
tstart=0
tend= 1500
trange=np.array([tstart,tend])
N=tend*1+1
tspan=np.linspace(tstart,tend,N)

# Fig 4 rebuild
fig = plt.figure(figsize=(12,9))
ax = plt.axes(projection ='3d')

C8_star = np.linspace(0, 3000,30 )
x0 = np.zeros(8)
x0[0] = 120000 # C8
x0[2] = 18000 # C3
x0[4] = 40000 # IAP
x0[6] = 40000 # BAR
for i in C8_star:
    x0[1] = i
    #print(x0)
    sol=inte.solve_ivp(odes,
        trange, x0, t_eval=tspan, args=(k,k_neg), method='LSODA')
    ax.plot3D(tspan, i*np.ones(N), sol.y[3,:], 'g')
```

```
    #print(sol.y[3,:])
ax.set_title('')
ax.set_xlabel('t')
ax.set_ylabel('C8* input')
ax.set_zlabel('C3*')
ax.set_ylim(3000,0)
ax.view_init(25, 135)
```

6.2 Code used for Extending the model

```
import numpy as np
import scipy.integrate as inte
import sympy as sp
import matplotlib.pyplot as plt

# initialization of ODE functions
def odes(t, x, k, k_neg):
    v1=k[0]*x[1]*x[2]
    v2=k[1]*x[0]*x[3]
    v3=k[2]*x[3]*x[4]-k_neg[2]*x[5]
    v4=k[3]*x[3]*x[4]
    v5=k[4]*x[1]
    v6=k[5]*x[3]
    v7=k[6]*x[5]
    v8=k[7]*x[4]-k_neg[7]
    v9=k[8]*x[0]-k_neg[8]
    v10=k[9]*x[2]-k_neg[9]
    v11=k[10]*x[1]*x[6]-k_neg[10]*x[7]
    v12=k[11]*x[6]-k_neg[11]
```

```
    v13=k[12]*x[7]
    v14 = k[13]*x[8]*x[1]
    v15 = k[14]*x[8] - k_neg[14]
    v16 = k[15]*x[9]*x[4] - k_neg[15]*x[10]
    v17 = k[16]*x[9]
    v18 = k[17]*x[10]
    v19 = k[18]*x[2]*x[9]



    dC8dt = -v2-v9 #C8
    dC8sdt = v2-v5-v11 #C8*
    dC3dt = -v1-v10-v19  #C3
    dC3sdt = v1-v3-v6+v19 #C3*
    dIAPdt = -v3-v4-v8-v16 # IAP
    dIAPsdt = v3-v7 # C3*~IAP
    dBARdt = -v11-v12 # BAR
    dBARsdt = v11-v13 # C8*~BAR
    dC9dt = -v14 - v15 #C9
    dC9sdt = v14-v16-v17 #C9*
    dC9sIAPdt = v16 - v18 #C9*~IAP

    return np.array([dC8dt,dC8sdt,dC3dt,dC3sdt,
                    dIAPdt,dIAPsdt,dBARdt,dBARsdt, dC9dt, dC9sdt,
                     dC9sIAPdt])

k = np.zeros(19)
k[0]=5.8*(10**-5)
```

```
k[1]=10**-5
k[2]=5*(10**-4)
k[3]=3*(10**-4)
k[4]=5.8*(10**-3)
k[5]=5.8*(10**-3)
k[6]=1.73*(10**-2)
k[7]=1.16*(10**-2)
k[8]=3.9*(10**-3)
k[9]=3.9*(10**-3)
k[10]=5*(10**-4)
k[11]=10**-3
k[12]=1.16*(10**-2)

k[13] = 10**-5
k[14] = 1.8*(10**-2)
k[15] = 3.4*(10**-4)
k[16] = 5.8*(10**-3)
k[17] = 7*(10**-3)
k[18] = 2e-5



k_neg = np.zeros(19)
k_neg[2]=0.21
k_neg[7]=464
k_neg[8]=507
k_neg[9]=81.9
k_neg[10]=0.21
k_neg[11]=40
```

```
k_neg[14] = 3
k_neg[15] = 3

# tspan
tstart=0
tend=1500
trange=np.array([tstart,tend])
N=tend*1+1
tspan=np.linspace(tstart,tend,N)

# Fig 4 rebuild
fig = plt.figure(figsize=(12,9))
ax = plt.axes(projection ='3d')

C8_star = np.linspace(0, 3000,20)
x0 = np.zeros(11)
x0[0] = 120000 # C8
x0[2] = 18000# C3
x0[4] = 40000 # IAP
x0[6] = 40000 # BAR
x0[8] = 100*1000 #C9 #varied for three different plots

for i in C8_star:
    x0[1] = i
    #print(x0)
    sol=inte.solve_ivp(odes,
        trange, x0, t_eval=tspan, args=(k,k_neg), method='LSODA')
```

```
        ax.plot3D(tspan, i*np.ones(N), sol.y[3,:], 'g')
        #print(sol.y[3,:])
    ax.set_title('')
    ax.set_xlabel('t')
    ax.set_ylabel('C8* input')
    ax.set_zlabel('C3*')
    ax.set_ylim(3000,0)
    ax.view_init(25, 135)
```

References

[AMVL+21] Fentaw Abegaz, Anne-Claire M. F. Martines, Marcel A. Vieira-Lara, Melany Rios-Morales, Dirk-Jan Reijngoud, Ernst C. Wit, and Barbara M. Bakker. Bistability in fatty-acid oxidation resulting from substrate inhibition. *PLoS Comput Biol*, 17(8), 2021.

[ECG+04] Thomas Eissing, Holger Conzelmann, Ernst D. Gilles, Frank Allgöwer, Eric Bullinger, and Peter Scheurich. Bistability analyses of a caspase activation model for receptor-induced apoptosis*. *Journal of Biological Chemistry*, 279(35):36892–36897, 2004.

[Elm07] Susan Elmore. Apoptosis: A review of programmed cell death. *Sage Journals*, 35(4):495–516, 2007.

[FHRSC05] Ting-Jun Fan, Li-Hui Han, and Jin Liang Ri-Shan Cong. Caspase family proteases and apoptosis. *Acta Biochimica et Biophysica Sinica*, 37(11):719–727, 2005.

[SBB+02] Xiao-Ming Sun, Shawn B. Bratton, Michael Butterworth, Marion MacFarlane, and Gerald M. Cohen. Bcl-2 and bcl-xl inhibit cd95-mediated

apoptosis by preventing mitochondrial release of smac/diablo and subsequent inactivation of x-linked inhibitor-of-apoptosis protein*. *Journal of Biological Chemistry*, 277(13):11345–11351, 2002.

[SJS+98] Henning R. Stennicke, Juliane M. Jurgensmeier, Hwain Shin, Quinn Deveraux, Beni B. Wolf, Xiaohe Yangi, Qiao Zhou, H. Michael Ellerby, Lisa M. Ellerby, Dale Bredesen, Douglas R. Green, John C. Reed, Christopher J. Froelichi, and Guy S. Salvesen. Pro-caspase-3 is a major physiologic target of caspase-8. *Journal of Biological Chemistry*, 273(42):27084–27090, 1998.

[SVG+04] Maya Saleh, John P. Vaillancourt, Rona K. Graham, Matthew Huyck, Srinivasa M. Srinivasula, Emad S. Alnemri, Martin H. Steinberg, Vikki Nolan, Clinton T. Baldwin, Richard S. Hotchkiss, Timothy G. Buchman, Barbara A. Zehnbauer, Michael R. Hayden, Lindsay A. Farrer, Sophie Roy, and Donald W. Nicholson. Differential modulation of endotoxin responsiveness by human caspase-12 polymorphisms. *Nature*, 429:75–79, 2004.

THE JOURNAL OF BIOLOGICAL CHEMISTRY
Vol. 279, No. 35, Issue of August 27, pp. 36892–36897, 2004
Printed in U.S.A.

Bistability Analyses of a Caspase Activation Model for Receptor-induced Apoptosis*

Received for publication, May 3, 2004, and in revised form, June 18, 2004
Published, JBC Papers in Press, June 18, 2004, DOI 10.1074/jbc.M404893200

Thomas Eissing‡§, Holger Conzelmann§¶, Ernst D. Gilles¶‖, Frank Allgöwer‡, Eric Bullinger‡, and Peter Scheurich‡‡**

*From the ‡Institute for Systems Theory in Engineering, University of Stuttgart, Pfaffenwaldring 9, 70550 Stuttgart, Germany, the ¶Institute for System Dynamics and Control, University of Stuttgart, Pfaffenwaldring 9, 70550 Stuttgart, Germany, the ‖Max Planck Institute for Dynamics of Complex Technical Systems, Sandtorstr. 1, 39106 Magdeburg, Germany, and the **Institute for Cell Biology and Immunology, University of Stuttgart, Allmandring 31, 70569 Stuttgart, Germany*

Apoptosis is an important physiological process crucially involved in development and homeostasis of multicellular organisms. Although the major signaling pathways have been unraveled, a detailed mechanistic understanding of the complex underlying network remains elusive. We have translated here the current knowledge of the molecular mechanisms of the death-receptor-activated caspase cascade into a mathematical model. A reduction down to the apoptotic core machinery enables the application of analytical mathematical methods to evaluate the system behavior within a wide range of parameters. Using parameter values from the literature, the model reveals an unstable status of survival indicating the need for further control. Based on recent publications we tested one additional regulatory mechanism at the level of initiator caspase activation and demonstrated that the resulting system displays desired characteristics such as bistability. In addition, the results from our model studies allowed us to reconcile the fast kinetics of caspase 3 activation observed at the single cell level with the much slower kinetics found at the level of a cell population.

Apoptosis is a genetically defined major form of programmed cell death enabling the organism to remove unwanted cells, *e.g.* during embryonal development and after immune responses, to select educated immune cells and to eliminate virally infected and transformed cells (1, 2). Enhanced or inhibited apoptotic cell death can be involved in severe pathological alterations, including developmental defects, autoimmune diseases, neurodegeneration, or cancer. Extrinsic and intrinsic apoptotic pathways can be distinguished, although partly employing overlapping signal transduction pathways. A hallmark of the ongoing apoptotic process is the activation of a family of aspartate-directed cysteine proteases, the caspases. Caspases are produced as proenzymes and become activated upon cleavage (3). Activation of caspases finally dismantles the cells via the cleavage of important regulatory and structural proteins and enables phagocytic removal of the dying cell (4). A simplified outline of the extrinsic pathway of apoptosis induction after death receptor stimulation is depicted in Fig. 1.

Mathematical modeling and systems theory can provide valuable tools to get insight into complex dynamical systems, to test hypotheses, and to identify weak points (5, 6). Previous modeling approaches in apoptosis focused on the extrinsically triggered pathways, resulting in complex models (7, 8). The model parameters were fitted to data derived from cell population studies showing caspase activation in a range from 30 min to several hours. These models can describe and nicely illustrate certain aspects of the signal transduction pathway. However, more recent experimental results performed at the single cell level show that the majority of caspases are activated within a very short time interval (<15 min) (9–12).

Obviously, the single cell level is relevant for a mechanistic understanding. With the focus on receptor-induced apoptosis, we used Monte Carlo methods to look for parameter domains that enable an appropriate description of apoptosis induction in a single cell (model based on Fig. 1, data not shown). The obtained results revealed an unexpected responsiveness of the system toward minute initiator caspase activation if required to act rapidly. This behavior of the model was caused by the caspase cascade that represents the main signaling route in so-called type I cells (13) (see Fig. 1, *yellow background*). We therefore translated the current picture of the extrinsically triggered caspase cascade in a very elementary form into a mathematical model enabling a thorough investigation through the application of analytical methods. Our results showed that within large parameter ranges, including values from the literature, this straightforward model structure is unable to appropriately describe the expected behavior that can be deduced from experimental data. We then showed a way of extending our model structure to reconcile these observed differences and presented a model now able to describe key characteristics like a fast execution phase and bistability. In addition, results from our model studies show a way to reconcile the fast kinetics of caspase 3 activation observed at the single cell level with the much slower kinetics found at the level of a cell population in terms of understanding and modeling.

EXPERIMENTAL PROCEDURES

The Mathematical Model—For each reaction considered under "Results" one reaction rate can be deduced (v_1–v_{13}). The cleavage reactions (1, 2, and 4) are treated as being irreversible, and it is assumed that the intermediary cleavage products ("enzyme-substrate complexes") only achieve very low levels and can thus be eliminated as reasonable estimations that have been confirmed by simulation experiments (data not shown). The reaction rate equations are deduced according to the law of mass action, which we here consider prior to other kinetic approaches, like Michaelis-Menten kinetics, although theoretical con-

* This work was supported by Deutsche Forschungsgemeinschaft, Sonderforschungsbereich 495, project D2. The costs of publication of this article were defrayed in part by the payment of page charges. This article must therefore be hereby marked "*advertisement*" in accordance with 18 U.S.C. Section 1734 solely to indicate this fact.

§ Both authors contributed equally to this work.

‡‡ To whom correspondence should be addressed. Tel.: 49-711-685-6987; Fax: 49-711-685-7484; E-mail: Peter.Scheurich@izi.uni-stuttgart.de.

siderations show that the results would be very similar in our case. From this, molecular balances can be derived for each considered molecular species resulting in a system of ordinary differential equations (see Equations 1–8). Two different model structures are considered in greater detail during this study. The basic model includes the reactions 1–10 and translates into the Equations 1–6 (not including v_{11} in Equation 2). The extended model hypothesis includes all reactions and translates into the complete equation system where $v_1 = k_1[C8^*]\cdot[C3]$, $v_2 = k_2[C3^*]\cdot[C8]$, $v_3 = k_3[C3^*]\cdot[IAP] - k_{-3}[iC3^* \sim IAP]$, $v_4 = k_4[C3^*]\cdot[IAP]$, $v_5 = k_5[C8^*]$, $v_6 = k_6[C3^*]$ $v_7 = k_7[iC3^* \sim IAP]$, $v_8 = k_8[IAP] - k_{-8}$, $v_9 = k_9[C8] - k_{-9}$, $v_{10} = k_{10}[C3] - k_{-10}$, $v_{11} = k_{11}[C8^*]\cdot[BAR] - k_{-11}[iC8^* \sim BAR]$, $v_{12} = k_{12}[BAR] - k_{-12}$, and $v_{13} = k_{13}[iC8^* \sim BAR]$.

$$\frac{d[C8]}{dt} = -v_2 - v_9 \quad \text{(Eq. 1)}$$

$$\frac{d[C8^*]}{dt} = v_2 - v_5(-v_{11}) \quad \text{(Eq. 2)}$$

$$\frac{d[C3]}{dt} = -v_1 - v_{10} \quad \text{(Eq. 3)}$$

$$\frac{d[C3^*]}{dt} = v_1 - v_3 - v_6 \quad \text{(Eq. 4)}$$

$$\frac{d[IAP]}{dt} = -v_3 - v_4 - v_8 \quad \text{(Eq. 5)}$$

$$\frac{d[C3^* \sim IAP]}{dt} = v_3 - v_7 \quad \text{(Eq. 6)}$$

$$\frac{d[BAR]}{dt} = -v_{11} - v_{12} \quad \text{(Eq. 7)}$$

$$\frac{d[C8^* \sim BAR]}{dt} = v_{11} - v_{13} \quad \text{(Eq. 8)}$$

The models were implemented in both Matlab (for simulation experiments) and Mathematica (for analytical analysis).

Initial Conditions, Parameters, and Units—The average concentrations in an unstimulated cell (*i.e.* initial conditions) of caspase 8 and 3 were quantified in HeLa cells to be 130,000 and 21,000 molecules/cell, respectively, using quantitative Western blot analyses.[1] The average concentration of IAP(s)[2] was estimated to be 40,000 molecules/cell. Other reported concentrations are 30, 200, and 30 nM for caspase 8, caspase 3, and XIAP, respectively (14, 15). Estimating a cell volume of 1 picoliter shows that 600 molecules/cell = 1 nM. Accordingly, these values are roughly in the same order of magnitude and were used as initial concentrations. The other compounds were considered not to be present in the absence of a stimulus. In the extended model, the concentration of the newly introduced molecule BAR was assumed to be 40,000 molecules/cell. We consider the unit molecules/cell more illustrative for cellular concentrations than the unit molar, but on the other hand we prefer and use units such as $M^{-1}\ s^{-1}$ for the K_m/k_{cat} ratios.

Table I lists the parameters as used in the "single set" simulations (unless indicated otherwise). The respective values are also provided in more common units (in brackets). For the reactions 3 and 5–10 the parameter values were taken from literature as stated in the text. The respective references are summarized in Table II. For the reactions 1, 2, and 4 values were chosen that are in accordance with the desired kinetics and the requirement for bistability (as deduced from bifurcation analyses). The values for reaction 11 were fixed under the assumption of a similar binding affinity as reported for reaction 3. The values for the reactions 12 and 13 represent estimated turnover rates.

Steady State Derivation—The steady states were derived under the steady state condition $dy/dt = 0$ (for all compound concentrations y). A consecutive elimination of variables leads to a polynomial in $C3^*$, whose solutions present the steady state concentrations of $C3^*$ from which the steady state concentrations of the other molecular species can be derived. The life steady state can be factored out leaving a quadratic equation of the general form $ax^2 + bx + c = 0$ for the basic model and a fourth-order polynomial for the extended model. The quadratic formula was used to construct the *green* ($b^2 = 4ac$; saddle-node bifurcation manifold) and the *blue* ($-b/a = 0$) area in Fig. 3. Interestingly, the coefficient c is the same as the coefficient c derived in the stability analysis (see below).

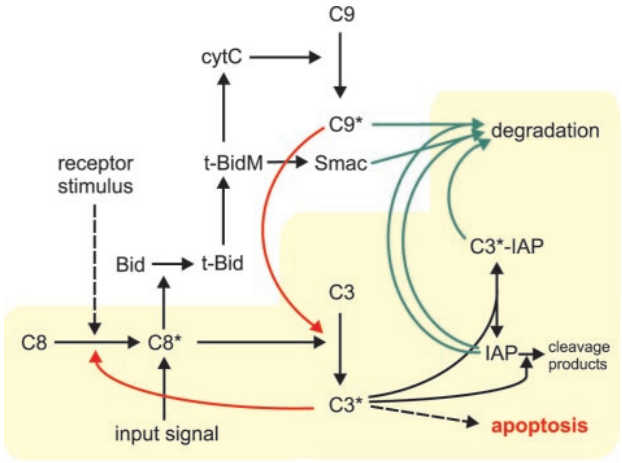

FIG. 1. **Outline of apoptotic pathways downstream of death receptors.** Initially, partial activation of caspase 8 (*C8**, the active status of caspases is indicated by an *asterisk*) is mediated by death receptor stimulation. C8* can cleave and activate caspase 3 (*C3*) directly but also cleaves Bid to release t-Bid. Mitochondrial t-Bid (*t-BidM*) leads to the release of cytochrome *c* (*cytC*) and Smac/DIABLO (*Smac*). Caspase 9 (*C9*) is activated by *cytC* and activates *C3*. *C3** can activate residual *C8* in a feedback loop. *C9** and *C3** can be inhibited by *IAP* molecules and subsequently fed into proteasomal degradation. Mitochondrially released Smac competes with the caspases for IAP binding and degradation.

Stability Analysis—For the life steady state one can construct the characteristic polynomial $\det(\lambda I - A) = 0$. Here, det refers to the determinant, λ represents the eigenvalues, I represents the identity matrix, and A represents the Jacobian matrix evaluated at the life steady state. For the non-linear ordinary differential equation system to be locally (asymptotically) stable, all eigenvalues need to have negative real parts. The Hurwitz criterion provides conditions for stability based on the coefficients of the characteristic polynomial. The most restrictive for the basic model is that the coefficient c (below) is positive, which was also used to construct the *red* area shown in Fig. 3 (transcritical bifurcation manifold). The stability of the steady states other than the life steady state were evaluated numerically, $c = k_5(IAP\ k_3\ k_7 + k_6(k_7 + k_{-3})) - C3\ C8\ k_1\ k_2(k_7 + k_{-3})$.

Deriving an Input Distribution—We assume a population behavior as depicted in Fig. 5*A*, which can be interpreted as a probability distribution. We further assume that 100% of caspase activation corresponds to 100% cell death, *i.e.* caspase 3 becomes significantly activated in every cell within the population. Furthermore, based on the simulations of the deterministic single cell model described in Fig. 4, we can describe the maximal caspase 3 activation as a function of *C8** input. Hereby we assume the maximal caspase activation to define the time point of cell death. This correlates the stochastic time point of cell death to a stochastic input signal for the single cells within a population. From the original distribution of Fig. 5*A* we thus obtain a distribution of cell death probability as a function of input activation. The corresponding probability density function can be derived by differentiation as shown in Fig. 5*B*.

RESULTS

The Biology of the Model System—The type I cell-like (13) model (called basic model hereafter) was constructed with the purpose of being as uncomplicated as possible without neglecting essential steps concerning our analyses (see below), *i.e.* simplifications represent conservative estimations. As a model input we use a pulse of activated caspase 8, which is produced by the death-inducing signaling complex formed at the membrane after death receptor stimulation (16) (although the initial steps seem to be more complex in the case of TNFR1 (17)). The model is outlined in Fig. 1 (*yellow background*) and contains the following reactions:

[1] T. Eissing, H. Conzelmann, E. D. Gilles, F. Allgöwer, E. Bullinger, and P. Scheurich, unpublished data.

[2] The abbreviations used are: IAP, inhibitor of apoptosis protein; BAR, bifunctional apoptosis regulator; CARP, caspase 8- and 10-associated RING proteins; C*n*, pro-caspase *n*; C*n**, activated caspase *n*.

TABLE I
Simulation parameters

Parameter values as used in the single set simulation experiments are given (mo = molecules). In parentheses the values are shown in more common units to enable direct comparison with literature values presented in Table II. For further information see "Experimental Procedures."

	Value	Unit		Value	Unit
k_1	$5.8{\cdot}10^{-5}$ ($5.8{\cdot}10^{5}$)	cell·min^{-1}·mo^{-1} (M^{-1} s^{-1})	k_{-1}	0	
k_2	10^{-5} (10^{5})	cell·min^{-1}·mo^{-1} (M^{-1} s^{-1})	k_{-2}	0	
k_3	$5{\cdot}10^{-4}$ ($5{\cdot}10^{6}$)	cell·min^{-1}·mo^{-1} (M^{-1} s^{-1})	k_{-3}	0.21 (0.035)	min^{-1} (s^{-1})
k_4	$3{\cdot}10^{-4}$ ($3{\cdot}10^{6}$)	cell·min^{-1}·mo^{-1} (M^{-1} s^{-1})	k_{-4}	0	
k_5	$5.8{\cdot}10^{-3}$ (120)	min^{-1} (min)	k_{-5}	0	
k_6	$5.8{\cdot}10^{-3}$ (120)	min^{-1} (min)	k_{-6}	0	
k_7	$1.73{\cdot}10^{-2}$ (40)	min^{-1} (min)	k_{-7}	0	
k_8	$1.16{\cdot}10^{-2}$ (60)	min^{-1} (min)	k_{-8}	464 ($1.3{\cdot}10^{-11}$)	mo·cell^{-1}·min^{-1} (M·s^{-1})
k_9	$3.9{\cdot}10^{-3}$ (180)	min^{-1} (min)	k_{-9}	507 ($1.4{\cdot}10^{-11}$)	mo·cell^{-1}·min^{-1} (M·s^{-1})
k_{10}	$3.9{\cdot}10^{-3}$ (180)	min^{-1} (min)	k_{-10}	81.9 ($2.3{\cdot}10^{-12}$)	mo·cell^{-1}·min^{-1} (M·s^{-1})
k_{11}	$5{\cdot}10^{-4}$ ($5{\cdot}10^{6}$)	cell·min^{-1}·mo^{-1} (M^{-1} s^{-1})	k_{-11}	0.21 (0.035)	min^{-1} (s^{-1})
k_{12}	10^{-3} (693)	min^{-1} (min)	k_{-12}	40 ($1.1{\cdot}10^{-12}$)	mo·cell^{-1}·min^{-1} (M·s^{-1})
k_{13}	$1.16{\cdot}10^{-2}$ (60)	min^{-1} (min)	k_{-13}	0	

$$C8^* + C3 \rightarrow C8^* + C3^*$$

REACTION 1

$$C8 + C3^* \rightarrow C8^* + C3^*$$

REACTION 2

$$C3^* + IAP \leftrightarrow iC3^* \sim IAP$$

REACTION 3

$$C3^* + IAP \rightarrow C3^*$$

REACTION 4

Pro-caspase 3 (*C*3, standing for the executioner caspases in general, *e.g.* caspases 3, 6, and 7) is cleaved and activated by activated caspase 8 (14, 18) (*C*8*; standing for both initiator caspases, caspases 8 and 10) (Reaction 1). Activated caspase 3 (*C*3*) acts in terms of a positive feedback loop onto pro-caspase 8 (C8) (19–21) (Reaction 2). Here we neglect the presumably amplifying effect of caspase 6 within this feedback loop. Activated caspase 3 binds to and is inactivated by XIAP, here for simplicity termed IAP, as cIAP-1 and cIAP-2 also have the capacity to block caspase 3, although with less efficiency (22, 23). IAP-bound activated caspase 3 may form a pool (Reaction 3), but, in parallel, IAP molecules can be cleaved by the activated caspase 3 (Reaction 4). The cleavage products of XIAP have been described to exert only minor effects on caspase 3 (24), so these are neglected. Also, the two cleaved forms of caspase 3 are not distinguished, as both have been described to possess similar catalytic activities (15). Furthermore, activated caspases, as well as activated caspase 3 complexed with IAPs, are continuously degraded and pro-caspases and IAPs are subjected to a turnover (Reactions 5–10, degradation and turnover reactions detailed under "Experimental Procedures"). We thus obtain a system of six ordinary differential equations as detailed under "Experimental Procedures."

Bistability and Apoptosis—Several signal transduction pathways governing cell fate decisions have experimentally and theoretically been shown to display a bistable behavior (25–27). Bistability is also an obvious and mandatory property of the apoptotic machinery, as the status "alive" must be stable and resistant toward minor accidental trigger signals (*i.e.* "noise") (28). Also, caspases are known to possess zymogenicity (18) and partial activation is observed in some physiological processes (29). However, if the apoptotic initiation signal is beyond a certain threshold, the cell must irreversibly enter the pathway to develop apoptosis. In the following, we use this information in a reverse engineering manner (6) and take bistability as an "essential condition" to evaluate possible models with respect to this expected behavior.

The Basic Model Shows an Unstable Life Steady State—Solving the equation system of our basic model under steady state conditions reveals three steady states. One of these, the "life steady state," corresponds to the initial conditions in which the system remains without an external trigger, *i.e.* without initial caspase 8 activation. This was expected because our model parameters defining the new synthesis of molecules had been chosen to balance their degradation, and additional influences were neglected. The stability of the steady state provides information about the system behavior close to that steady state, indicating the response to very minor activating input signals. If the steady state is stable, the system will return to its original steady state, provided the perturbations are small enough, which is a situation expected for our model.

The stability of a steady state can be evaluated using the Hurwitz criterion, which is well established in systems theory (see "Experimental Procedures"). The point where the stability properties change, *i.e.* the bifurcation point, provides insight into the qualitative system behavior for certain parameter ranges. We introduced fixed parameter values for all reaction rates except for Reaction 1 (Table I) and found that the life steady state is only stable for k_1 values below $\sim 3.2 \times 10^3$ M^{-1} s^{-1}, a value more than 300 times lower than reported in literature (14, 18) (the situation is illustrated in Fig. 2). Fig. 3 shows the bifurcation point (*red* area) in dependence of three parameter classes with fixed ratios in each class. The parameter combination that can be deduced from literature (Fig. 3, *yellow dot*) is far away from those combinations enabling a stable life steady state (Fig. 3, below the *red area*). To further confirm our results, we conducted several million simulations with small inputs and random sets of parameters taken from the parameter ranges shown in Table II. All combinations resulted in significant caspase activation with very small input signals (*i.e.* an unstable life steady state), although the onset time varied greatly (data not shown).

Bistability within a Small Parameter Domain—The two additional steady states besides the life steady state provide further information. Theoretically, one additional steady state within the positive concentration range is sufficient to achieve bistability (because phenomena other than an unstable steady state could separate the two stable steady states). However, in our model this configuration is only possible above the *red* area in Fig. 3 (see "Experimental Procedures") and for that setting the life steady state is unstable. Accordingly, bistability is only possible if both additional steady states are within the positive concentration range (Fig. 3, above the *blue area*). Another restriction is imposed by our biological system, because the solutions must contain real numbers (Fig. 3, above the *green*

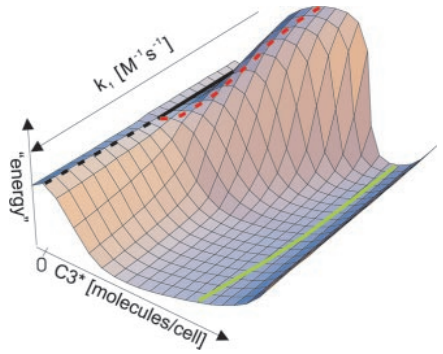

FIG. 2. **Bifurcation illustration.** A steady state implies that the concentrations of the compounds within the system do not change over time. If we start at close by concentrations, the system will move back into the steady state if it is stable but move away if it is unstable. Here the steady states and their stability properties dependent on the reaction rate k_1 are illustrated schematically with the other parameters kept constant. The third coordinate can be envisioned as energy and was introduced to add plasticity. *Solid lines* indicate stable steady states, and *dashed lines* indicate unstable steady states. For small values of k_1 we find a landscape of a bistable system with a stable life steady state (*black line*), a stable apoptotic steady state (*green line*), and a third unstable steady state separating the two areas of attraction (*red line*). When the parameter k_1 increases, the landscape changes as the unstable separating steady state meets with the stable life steady state. At this bifurcation point the two steady states exchange their stability properties, and the formerly separating steady state vanishes into the biologically irrelevant negative concentration area. Thus, for larger values of k_1 the life steady state is unstable and the apoptotic steady state is stable and attractive in the whole positive concentration area.

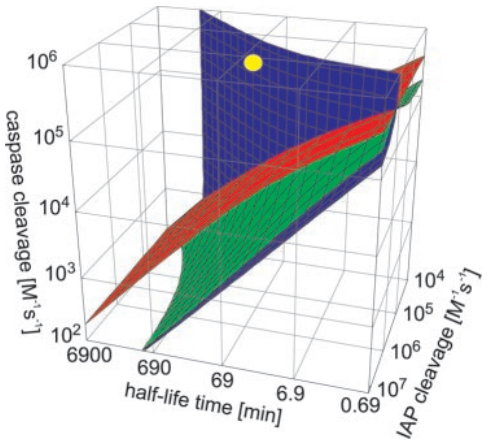

FIG. 3. **(Bi-)Stability analysis.** Stability aspects of the basic model were evaluated over wide parameter ranges. For the three-dimensional visualization the following parameter ratios were chosen as axes, for caspase activation, $k_1 = 2{\cdot}k_2$; for half-life time, $k_7 = k_8 = 2{\cdot}k_5 = 2{\cdot}k_6 = 4{\cdot}k_9 = 4{\cdot}k_{10}$; and for IAP cleavage, k_4; v_3 was fixed according to literature values. The *yellow dot* indicates values as expected from literature data (although the IAP cleavage reaction parameter can only be estimated, see Table II). Above the *red area* no stable life steady state exists, below the *blue area* no second stable steady state within the positive concentration range can exist and below the *green area* the solutions are complex numbers. Thus, bistability requires parameter combinations below the *red* and above the *blue* and above the *green* areas.

area). Thus, bistability is only possible in a very restricted parameter area far away from values reported in literature (Fig. 3, *yellow dot*). In accordance with general considerations on this topic (25, 30) the feedback from caspase 3 onto caspase 8 is necessary for bistability (data not shown).

IAPs and Their Cleavage—Interestingly, by and large the stability of the life steady state seems to be independent of the IAP cleavage reaction (Fig. 3). This is not expected and indeed dynamic simulations show that, upon faster IAP cleavage, the onset of caspase activation is achieved more rapidly for parameter combinations where the life steady state is unstable (data not shown). However, for parameter combinations where the life steady state is stable, a slower reaction stabilizes the life steady state by enlargement of its area of attraction (globally stable without this reaction). This can be explained by the fact that we assumed higher concentrations of IAPs than that of caspase 3 to make a conservative estimation concerning the stability of the life steady state. If we assume lower numbers of IAP molecules, we can achieve bistability (which would also require the turnover of IAPs not to exceed that of caspases significantly) even in the absence of this cleavage reaction. However, the parameters in which a stable life steady state is possible would be even further away from those values reported in literature (data not shown). Together, the model indicates that the IAP cleavage reaction is important for a decisive switching.

Further analysis of the model reveals that apoptosis can only proceed after the IAP pool is exhausted, as otherwise most of the active caspase 3 molecules become neutralized (data not shown). As the binding of active caspase 3 to IAPs is a reversible reaction, a slower degradation of the complexes would elevate the levels of free active caspase 3 and therefore promote apoptosis. Thus, our results also argue for the view of IAPs as altruistic proteins sacrificing themselves to prevent cell death (31). In our investigations we did not change the initial concentrations to restrict the number of free parameters. However, in the mathematical formulas it can be seen that changing a parameter value has similar effects as changing an initial concentration, and so we have indirectly evaluated these influences as well.

Bistability through Model Extension—An inherent problem of the described basic model of caspase activation is that relatively fast activation kinetics must be realized to be consistent with parameter values from literature and observations in various experimental setups (9–12, 32, 33). On the other hand, only if the kinetics are slow will the system display the desired bistability. There are several possibilities explaining how a model extension could reconcile those facts as described under "Discussion." One possibility is a mechanism to inhibit active caspase 8. In fact, recent reports describe that activated caspase 8 can be functionally inactivated in mitochondrial membranes. There, the molecule BAR has been proposed to bind activated caspase 8 via its pseudodeath effector domain leading to effective neutralization of its proteolytic activity (34–37). We therefore introduced the molecule BAR into our model and assumed it to bind to activated caspase 8 with an affinity similar to XIAP binding to activated caspase 3 (23, 38). In addition, we introduced a normal turnover rate for the new compounds (see "Experimental Procedures").

The resulting system provides five steady states, two of which contain negative concentrations for the evaluated area and are thus not of interest. Importantly, stability of the life steady state of this extended model is possible with kinetic values close to those described in literature (illustrated in Fig. 2, bifurcation point at $k_1 \approx 5.9{\cdot}10^5\ \mathrm{M}^{-1}\ \mathrm{s}^{-1}$ for other parameters as shown in Table I). We performed simulations with input signals of different strength (Fig. 4), using a set of parameters where the system displays a bistable behavior (Table I). In each case, caspase activity remains low for a certain time, inversely proportional to the stimulus strength, followed by a steep rise in activity if the input exceeds the threshold (~75 molecules of activated caspase 8/cell). After reaching a maximum, caspase activity ceases again because of, it is our assumption, higher degradation rates for the activated caspases as compared with the production rates of the pro-caspases. Similar to the model without the molecule BAR, the IAPs again play a critical role. Only after the IAP and BAR pools have been exhausted, apoptosis can proceed (data not shown). Although the exact quan-

TABLE II
Unstability ranges

Parameter ranges that do not provide parameter combinations enabling a stable life steady state. The k_- column indicates whether a reaction (see "Experimental Procedures") is assumed to be reversible or not. If reversible, the values can be calculated with the help of the provided explanations. The last column also provides literature parameter values and the respective references.

	k_+min	k_+max	k_-	Explanations and refs.
	$M^{-1}\,s^{-1}$	$M^{-1}\,s^{-1}$	$M^{-1}\,s^{-1}$	
v_1	$3{\cdot}10^4$	$5{\cdot}10^6$	No	*In vitro* K_M/k_{cat} = 10^6 M^{-1} s^{-1} (14, 18)
v_2	$2{\cdot}10^4$	$5{\cdot}10^6$	No	*C*3* faster than *C*8* using fluorogenic substrates (18, 21, 45)
v_3	$1{\cdot}10^5$	$5{\cdot}10^6$	Yes	To obtain: *in vitro* K_i = 0.7 nM (23, 38)
v_4	$1{\cdot}10^3$	$5{\cdot}10^6$	No	Estimation
	$t_{1/2}$min (min)	$t_{1/2}$max (min)	k_- (M·s^{-1})	k_+ (min^{-1}) = ln2/$t_{1/2}$
v_5	30	300	No	
v_6	30	300	No	$t_{1/2}$ ~ 180 min for caspases; $t_{1/2}$ = 30–40 min for DIAP (31, 46)
v_7	30	300	No	
v_8	30	300	Yes	
v_9	60	500	Yes	Production rate to establish the initial concentration
v_{10}	60	500	Yes	

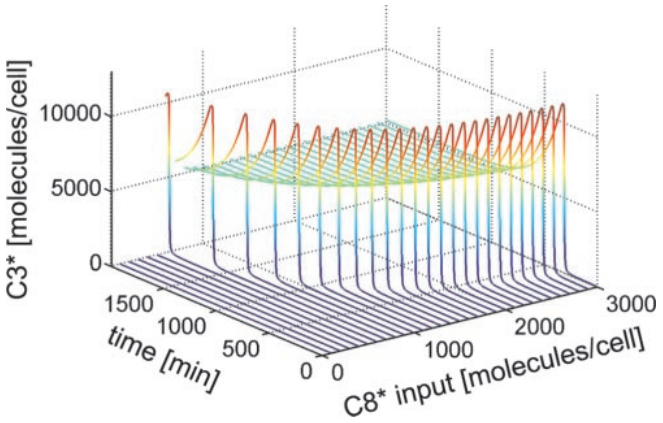

FIG. 4. **Bistable behavior of the extended model.** Simulation experiments with varying inputs (initial *C8** concentrations) and *C3** over time as output are shown. Above a certain input threshold (~75 molecules of C8*) the system becomes fully activated, whereas subthreshold activation results in recovery. The two stable steady states can be envisioned, with the life steady state corresponding to the *blue area* and the apoptotic steady state corresponding to the *green area* achieved after longer time periods.

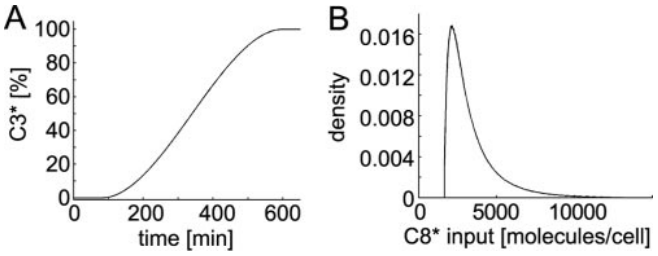

FIG. 5. **Reconciling single cell and populations kinetics.** *A*, an idealized time course of caspase 3 activation as observed at the population level. *B*, the density function of the input signal necessary to achieve the population behavior depicted in *A*, based on single cells behaving as described in the legend to Fig. 4.

titative behavior depends on the choice of parameters, these simulations display the desired characteristics like bistability and fast activation kinetics combined with prolonged lag phases, inversely related to the strength of the apoptotic trigger, as observed in experiments (9).

Reconciling Single Cell and Population Studies—The model derived here has the aim to reproduce certain aspects of apoptosis induction at the single cell level. However, most experimental studies have been performed using cell populations where effector-caspase activation is typically observed within a range of a few hours (13, 39, 40). Fig. 5*A* shows an example of a slow time course of effector-caspase activation. As described above, the strength of the apoptotic stimulus mainly translates into the delay between the apoptotic trigger and significant effector-caspase activation. Thus, different delay times because of the stochastic nature of biological systems enable small fast single-cell segments of caspase activation to integrate, forming an overall slow caspase activation at the macroscopic level. Fig. 5*B* shows the distribution of input signals into the extended BAR model (as described above) required to produce a population behavior as depicted in Fig. 5*A* (see "Experimental Procedures"). Although this approach is very simplified, it already reconciles single cell and population data and shows a way of combing both in terms of understanding and modeling.

DISCUSSION

In the past, systems theory has been mainly used to understand dynamic processes of technical structures, but recently it has been increasingly applied in biology (5, 6). Many articles focus on the mathematical modeling of aspects of the metabolism, where (quasi) steady state approximations can be used and the mere structure provides valuable information (41). The initiation and development of apoptosis, however, is a highly dynamic process where steady state approximations cannot be easily applied. We employed a reduced model to evaluate the principle behavior, but also took dynamic information into account using data from various sources trying to fuse them together with the help of our model. The class of biological systems exemplified here has not been evaluated previously with respect to bistability, although bistability can be shown for special classes of larger systems (30). Our results showed that (partly) analytic approaches for additional classes are feasible for larger systems than widely believed.

The present study analyzes the basic core reactions of caspase activation as they are accepted widely as occurring after death receptor activation (2, 3, 42). Because the molecular events occurring at the level of the receptor-induced signaling complex are only in part understood (13, 17), the input signal of the model is represented by a given number of molecules of activated initiator caspase (Fig. 1), excluding the pathways mediating initial caspase activation. This model, however, reveals no stable steady state in the life status, mainly because of the strong forward reaction of the caspase cleavage reactions, as such, containing a positive feedback loop. We therefore reduced further analyses to the reactions depicted in Fig. 1 on the *yellow background*, including the caspase activation reactions. Bifurcation analyses of this basic model reveal that it is capable of displaying the desired bistable behavior only within a narrow range of kinetic parameter values that are far from the

values reported in the literature. We thus considered possible modifications in the model structure, capable of reconciling the observed fast kinetics and tolerance to subthreshold stimuli. A common way in cell biology to achieve such a behavior is cooperativity (25), which could also be assumed to exist for caspases, as they are known to act as heterodimers. However, recent work (43) shows that the monomer is just as bioactive as the dimer, arguing against this possibility. Alternatively, one might suggest a mechanism where the kinetic constants are not altered, but where the amount of free active caspase is limited. Such mechanisms are well known to exist for caspases 3 and 9, where IAPs lower the effective concentration of active proteases. In addition, more recent reports describe the inhibitory molecule BAR, acting at the caspase 8 level (34–37)(see "Results"). Based on these data reported in the literature, we extended our basic model to include BAR, and the resulting model system displays the mandatory bistable behavior within a wide parameter range close to the kinetic parameter values reported in the literature. Moreover, this extended model now easily describes the fast activation kinetics of caspase activation in individual cells, combined with prolonged lag phases in agreement with experimental data (9). Although additional explanations for these long lag phases have been proposed recently (at least for tumor necrosis factor-induced apoptosis (17)), our studies demonstrated that caspase 8 capture/inactivation is a likely mechanistic explanation for the observed lag period followed by fast effector-caspase activation. Whereas this lag phase might be largely controlled at the level of the mitochondria in type II cells (9, 10), a similar behavior was also observed for type I cells, although initial activation of caspase 8 takes place immediately after stimulation (13, 16).

In fact, in a very recent publication (44) a new class of molecules has been described, termed caspase 8- and 10-associated RING proteins (CARPs), that are proposed to be novel caspase 8 and 10 inhibitors, acting similarly to the IAP proteins. In the light of the results from our studies, these experimental data underscore the necessity for an effective regulation at the level of initiator caspases in death-receptor-mediated apoptosis. Regarding the model system, the effects of direct caspase 8 inhibition and inactivation by CARPs or their capture at the mitochondrial membranes by BAR proteins are reasonably equivalent, as the mathematical model does not take into account processes of diffusion, and both mechanisms effectively lower the number of molecules of free active initiator caspase.

In experimental studies the activation of effector caspases both in type I as well as type II cell populations occurs gradually within a few hours (13, 39, 40), as schematically depicted in Fig. 5*A*. However, at the single cell level, rapid caspase 3 activation has been observed after a lag phase in the very same experimental setup (9–12). Using our extended model, we can easily reconcile the observed fast kinetics at the single cell level with the slower rates observed in cell populations. We showed here that the variation of the input signal strength within single cells, as depicted in Fig. 5*B*, results in slow kinetics at the population level as shown in Fig. 5*A*. The required stochastic input can be explained, for example, by different numbers of death receptors expressed in different cells, but also in a similar way by (or more likely in combination with) different numbers of BAR proteins, CARPs, and other molecules involved. The number of caspase 8 inhibitors, for example, strongly influences the threshold, as also observed in siRNA experiments against CARPs (44). Together, these results demonstrate that a strongly reduced model of complex signaling networks like the apoptotic machinery already allows testing and falsifying in comparison with experimental data, leading to a deeper insight into the control mechanisms of complex cellular responses.

Acknowledgments—We thank the Systems Biology Group Stuttgart and Harald Wajant for fruitful discussions.

REFERENCES

1. Leist, M., and Jaattela, M. (2001) *Nat. Rev. Mol. Cell. Biol.* **2,** 589–598
2. Hengartner, M. O. (2000) *Nature* **407,** 770–776
3. Thornberry, N. A., and Lazebnik, Y. (1998) *Science* **281,** 1312–1316
4. Savill, J., and Fadok, V. (2000) *Nature* **407,** 784–788
5. Kitano, H. (2002) *Nature* **420,** 206–210
6. Csete, M. E., and Doyle, J. C. (2002) *Science* **295,** 1664–1669
7. Fussenegger, M., Bailey, J. E., and Varner, J. (2000) *Nat. Biotechnol.* **18,** 768–774
8. Schöberl, B., Gilles, E. D., and Scheurich, P. (2001) in *Proceedings of the International Congress of Systems Biology, Pasadena, CA, November 4–7, 2001* (Yi, T.-M., Hucka, M., Morohashi, M., and Kitano, H., eds) pp. 158–167, Omnipress, Madison, WI
9. Rehm, M., Dussmann, H., Janicke, R. U., Tavare, J. M., Kogel, D., and Prehn, J. H. (2002) *J. Biol. Chem.* **277,** 24506–24514
10. Goldstein, J. C., Waterhouse, N. J., Juin, P., Evan, G. I., and Green, D. R. (2000) *Nat. Cell Biol.* **2,** 156–162
11. Luo, K. Q., Yu, V. C., Pu, Y., and Chang, D. C. (2003) *Biochem. Biophys. Res. Commun.* **304,** 217–222
12. Tyas, L., Brophy, V. A., Pope, A., Rivett, A. J., and Tavare, J. M. (2000) *EMBO Rep.* **1,** 266–270
13. Scaffidi, C., Fulda, S., Srinivasan, A., Friesen, C., Li, F., Tomaselli, K. J., Debatin, K. M., Krammer, P. H., and Peter, M. E. (1998) *EMBO J.* **17,** 1675–1687
14. Stennicke, H. R., Jurgensmeier, J. M., Shin, H., Deveraux, Q., Wolf, B. B., Yang, X., Zhou, Q., Ellerby, H. M., Ellerby, L. M., Bredesen, D., Green, D. R., Reed, J. C., Froelich, C. J., and Salvesen, G. S. (1998) *J. Biol. Chem.* **273,** 27084–27090
15. Sun, X. M., Bratton, S. B., Butterworth, M., MacFarlane, M., and Cohen, G. M. (2002) *J. Biol. Chem.* **277,** 11345–11351
16. Lavrik, I., Krueger, A., Schmitz, I., Baumann, S., Weyd, H., Krammer, P. H., and Kirchhoff, S. (2003) *Cell Death Differ.* **10,** 144–145
17. Micheau, O., and Tschopp, J. (2003) *Cell* **114,** 181–190
18. Stennicke, H. R., and Salvesen, G. S. (1999) *Cell Death Differ.* **6,** 1054–1059
19. Slee, E. A., Harte, M. T., Kluck, R. M., Wolf, B. B., Casiano, C. A., Newmeyer, D. D., Wang, H. G., Reed, J. C., Nicholson, D. W., Alnemri, E. S., Green, D. R., and Martin, S. J. (1999) *J. Cell Biol.* **144,** 281–292
20. Cowling, V., and Downward, J. (2002) *Cell Death Differ.* **9,** 1046–1056
21. Van de Craen, M., Declercq, W., Van den brande, I., Fiers, W., and Vandenabeele, P. (1999) *Cell Death Differ.* **6,** 1117–1124
22. Salvesen, G. S., and Duckett, C. S. (2002) *Nat. Rev. Mol. Cell. Biol.* **3,** 401–410
23. Ekert, P. G., Silke, J., and Vaux, D. L. (1999) *Cell Death Differ.* **6,** 1081–1086
24. Deveraux, Q. L., Leo, E., Stennicke, H. R., Welsh, K., Salvesen, G. S., and Reed, J. C. (1999) *EMBO J.* **18,** 5242–5251
25. Ferrell, J. E., and Xiong, W. (2001) *Chaos* **11,** 227–236
26. Ferrell, J. E., Jr. (2002) *Curr. Opin. Cell Biol.* **14,** 140–148
27. Xiong, W., and Ferrell, J. E., Jr. (2003) *Nature* **426,** 460–465
28. Tyson, J. J., Chen, K. C., and Novak, B. (2003) *Curr. Opin. Cell Biol.* **15,** 221–231
29. Newton, K., and Strasser, A. (2003) *Genes Dev.* **17,** 819–825
30. Angeli, D., Ferrell, J. E., Jr., and Sontag, E. D. (2004) *Proc. Natl. Acad. Sci. U. S. A.* **101,** 1822–1827
31. Ditzel, M., and Meier, P. (2002) *Trends Cell Biol.* **12,** 449–452
32. Krippner-Heidenreich, A., Tubing, F., Bryde, S., Willi, S., Zimmermann, G., and Scheurich, P. (2002) *J. Biol. Chem.* **277,** 44155–44163
33. Fladmark, K. E., Brustugun, O. T., Hovland, R., Boe, R., Gjertsen, B. T., Zhivotovsky, B., and Doskeland, S. O. (1999) *Cell Death Differ.* **6,** 1099–1108
34. Qin, Z. H., Wang, Y., Kikly, K. K., Sapp, E., Kegel, K. B., Aronin, N., and DiFiglia, M. (2001) *J. Biol. Chem.* **276,** 8079–8086
35. Zhang, H., Xu, Q., Krajewski, S., Krajewska, M., Xie, Z., Fuess, S., Kitada, S., Pawlowski, K., Godzik, A., and Reed, J. C. (2000) *Proc. Natl. Acad. Sci. U. S. A.* **97,** 2597–2602
36. Breckenridge, D. G., Nguyen, M., Kuppig, S., Reth, M., and Shore, G. C. (2002) *Proc. Natl. Acad. Sci. U. S. A.* **99,** 4331–4336
37. Stegh, A. H., Barnhart, B. C., Volkland, J., Algeciras-Schimnich, A., Ke, N., Reed, J. C., and Peter, M. E. (2002) *J. Biol. Chem.* **277,** 4351–4360
38. Deveraux, Q. L., Takahashi, R., Salvesen, G. S., and Reed, J. C. (1997) *Nature* **388,** 300–304
39. Fotin-Mleczek, M., Henkler, F., Samel, D., Reichwein, M., Hausser, A., Parmryd, I., Scheurich, P., Schmid, J. A., and Wajant, H. (2002) *J. Cell Sci.* **115,** 2757–2770
40. Hentze, H., Schmitz, I., Latta, M., Krueger, A., Krammer, P. H., and Wendel, A. (2002) *J. Biol. Chem.* **277,** 5588–5595
41. Stelling, J., Klamt, S., Bettenbrock, K., Schuster, S., and Gilles, E. D. (2002) *Nature* **420,** 190–193
42. Ashkenazi, A. (2002) *Nat. Rev. Cancer* **2,** 420–430
43. Donepudi, M., Mac Sweeney, A., Briand, C., and Grutter, M. G. (2003) *Mol. Cell* **11,** 543–549
44. McDonald, E. R., III, and El-Deiry, W. S. (2004) *Proc. Natl. Acad. Sci. U. S. A.* **101,** 6170–6175
45. Garcia-Calvo, M., Peterson, E. P., Rasper, D. M., Vaillancourt, J. P., Zamboni, R., Nicholson, D. W., and Thornberry, N. A. (1999) *Cell Death Differ.* **6,** 362–369
46. Yoo, S. J., Huh, J. R., Muro, I., Yu, H., Wang, L., Wang, S. L., Feldman, R. M., Clem, R. J., Muller, H. A., and Hay, B. A. (2002) *Nat. Cell Biol.* **4,** 416–424